Journal of Ceramic Processing Research. Vol. 15, No. 3, pp. 173~176 (2014)

J O U R N A L O F
Ceramic Processing Research

Synthesis and photoluminescence properties of $HEu(MoO_4)_2$ nanophosphor

Mizuki Watanabe[a], Kazuyoshi Uematsu[b], Sun Woog Kim[a], Kenji Toda[a,*] and Mineo Sato[b]
[a]*Graduate School of Science and Technology, Niigata University, 8050 Ikarashi 2-nocho, Niigata 950-2181, Japan*
[b]*Department of Chemistry and Chemical Engineering, Niigata University, 8050 Ikarashi 2-nocho, Niigata 950-2181, Japan*

The $HEu(MoO_4)_2$ nanophosphor was synthesized for the first time by the H^+-exchange of $KEu(MoO_4)_2$. The nanophosphor obtained in the present study maintain the triclinic $KEu(MoO_4)_2$ type structure in a single phase form with high crystallinity. The $HEu(MoO_4)_2$ phosphor has rod-like particle morphology (length 0.5-20 μm, diameter 50-400 nm). Both $HEu(MoO_4)_2$ powder and solution shows red emission due to the 4f-4f transition of Eu^{3+}.

Key words: Nano material, Molybdate phosphor, H^+ exchange, Soft chemistry.

Introduction

Recently, nanophosphors were actively investigated due to their potential applications in the flat panel displays, solar energy converters, optical amplifiers, electroluminescenct devices, photodiodes, bio-detectors, sensors, and color display. They are also significantly important material in the field of luminescence because they exhibit excellent optoelectronic properties [1-5]. Among these applications, solar energy converters have been received much attention during the last few decades [6-8]. The crystal Si solar cells were widely used on an industrial scale because of its low cost and high electrical conversion efficiency. However, the efficiency limit of crystal Si solar cells was approximately 30%, which is considered to be the mismatch between the incident solar photon spectrum and the energy band gap of silicon. In particular, silicon has low optical absorption below 500 nm (Fig. 1). Therefore, various schemes have been proposed to overcome this fundamental efficiency limit for the crystal Si solar cells [9-16]. Among these schemes, one way to surpass this limit is using a luminescence down-shifting process to absorb high-energy photons and re-emit them at longer wavelengths such that the photovoltaic device exhibits a significantly better response. Therefore, investigations have been devoted to search for new high efficiency down-conversion nanophosphors, which can show excellent optical absorption below 500 nm.

In this study, we have focused on triclinic alkali rare earth molybdate, $KEu(MoO_4)_2$ as a precursor, to synthesize emissive nanophosphor material for use in crystal Si solar cells, because the molybdate phosphors show excellent optical absorption below 500 nm, to which crystal Si solar cells are less sensitive. In addition, it is well known that molybdate nanophosphors are easily prepared by wet chemical routes without calcination because their crystallization temperatures are relatively lower than those of other oxide materials [17]. Furthermore, the triclinic $KEu(MoO_4)_2$ has suitable

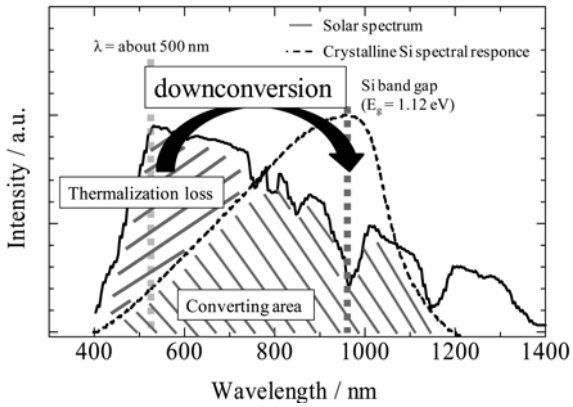

Fig. 1. Downconversion for crystalline Si solar cell.

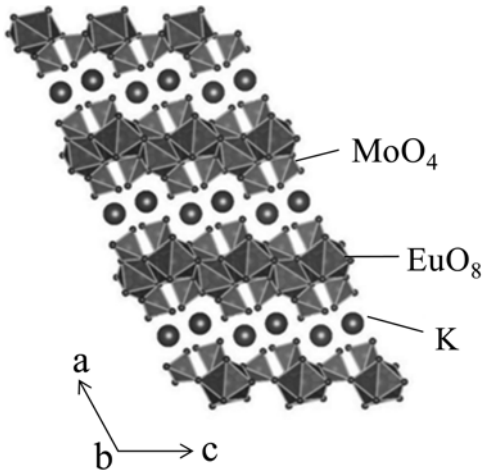

Fig. 2. The crystal structure of $KEu(MoO_4)_2$.

*Corresponding author:
Tel : +81-25-262-6771
Fax: +81-25-262-6771
E-mail: ktoda@eng.niigata-u.ac.jp

layer structure as illustrated in Figure 2 [18, 19], in which the EuO_8 polyhedron layer occupy cavities between two MoO_4 tetrahedron layers in the direction of the c-axis and the exchangeable potassium cations located between these $(Eu(MoO_4)_2)_n$ layers. This is indicates that K^+ ion in the $KEu(MoO_4)_2$ was easily exchanged with another ions by the ion-exchanging method, and it is expected to be controlled easily the particle size and morphology. However, to the best of our knowledge, it is no report on the successful ion-exchange of molybdate nanophosphor. In the present study, in contrast, we have successfully exchanged K^+ ion in the $KEu(MoO_4)_2$ with H^+ and synthesized the $HEu(MoO_4)_2$ nanophosphor with high luminescence efficiency by the ion-exchanging method and their particle morphology and luminescence properties have been investigated.

Experimental

$KEu(MoO_4)_2$ was synthesized by a conventional solid-state reaction method. A mixture of K_2CO_3, Eu_2O_3, and MoO_3 was mixed using a mortar with acetone, and then the mixture was calcined at 1000 ºC for 6 hrs in air. $HEu(MoO_4)_2$ was obtained by the H^+-exchange of $KEu(MoO_4)_2$ in 0.01 M aqueous HNO_3 solution (100 mL) at room temperature for 7 days. After stirring, the solution was isolated suction filtration with membrane filter (ADVANTEC MFS, INC., mixed cellulose ester, pore size: 0.45 μm, diameter: 47 mm). The sample was washed with deionized water for 12 hrs and then dried at 60 ºC for 12 hrs. The obtained powder ($HEu(MoO_4)_2$ powder) was redispersed in ion-exchanged water (pH = 7).

The obtained samples were characterized by X-ray powder diffraction (MX-Labo; Mac Science Ltd.) to identify the crystal structure and the sample composition was analyzed by X-ray fluorescence analysis (SII, SEA 1200VX). Morphology of the samples was characterized by means of scanning electron microscopy (SEM, Hitachi S-4300SD). The emission (PL) and excitation (PLE) spectra were measured at room temperature with a spectrofluorometer (Jasco Corp. FP-6500/6600), where the emission spectra were obtained for excitation at 467 nm, and excitation spectra were obtained for emission at 612 nm.

Results and Discussion

The composition of $KEu(MoO_4)_2$ was confirmed to be stoichiometric ratio by XRF analysis and the K^+ ion was not detected in the $HEu(MoO_4)_2$ sample after the H^+ exchange of $KEu(MoO_4)_2$, which indicates that K^+ ion in the $KEu(MoO_4)_2$ was successfully exchanged with H^+ ion. Figure 3 shows the powder XRD patterns of the precursor $KEu(MoO_4)_2$ powder and $HEu(MoO_4)_2$ powder prepared by the H^+ exchange of $KEu(MoO_4)_2$.

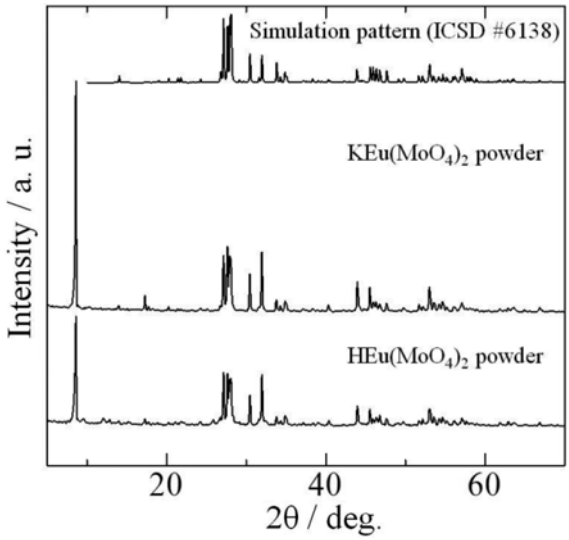

Fig. 3. XRD patterns of the precursor $KEu(MoO_4)_2$ powder and $HEu(MoO_4)_2$ powder.

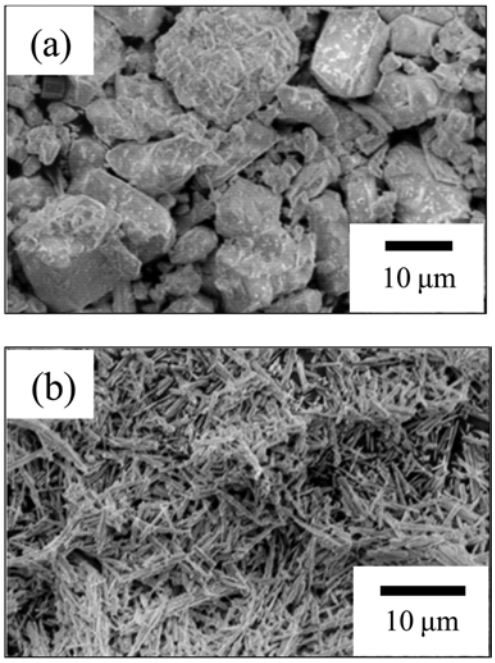

Fig. 4. SEM images of SEM images of (a) $KEu(MoO_4)_2$ and (b) $HEu(MoO_4)_2$ powders.

The powder XRD patterns of $KEu(MoO_4)_2$ and $HEu(MoO_4)_2$ were in good agreement with a single phase of triclinic $KEu(MoO_4)_2$ structure. These results indicate that the crystal structure of $KEu(MoO_4)_2$ is still well maintained after proton-exchange.

Figure 4 shows the SEM images of $KEu(MoO_4)_2$ and $HEu(MoO_4)_2$. The $KEu(MoO_4)_2$ phosphor has a granular particle morphology and the average particle size was 10 μm. On the contrary, the $HEu(MoO_4)_2$ phosphor has rod-like particle morphology and the nanorod particle are 0.5-20 μm in length, and most have outer diameters ranging from 50 to 400 nm. These results indicate that the particle size and morphology of

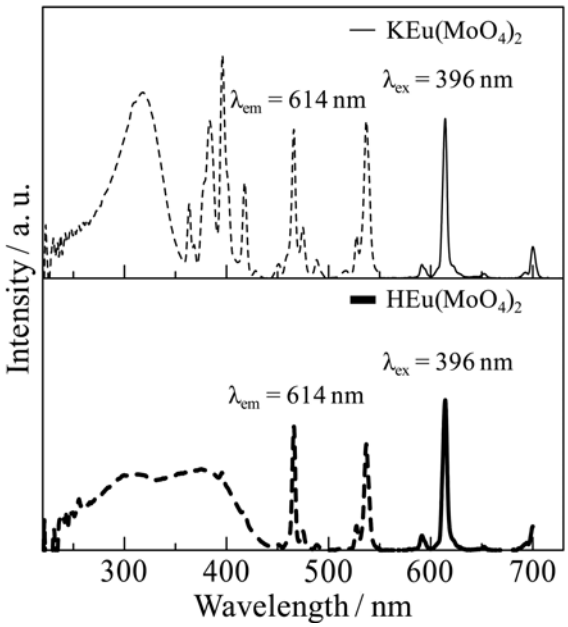

Fig. 5. Photoluminescence excitation and emission spectra of $KEu(MoO_4)_2$ and $HEu(MoO_4)_2$ powders.

$KEu(MoO_4)_2$ were successfully changed by the H^+-exchanging in the K^+ site, although the sample after H^+-exchanging was maintain layered crystal structure. However, unfortunately, we do not have any direct evidence to explain the mechanism of the particle morphology change with H^+-exchanging. Therefore, further studies are necessary to unveil the mechanism of the particle morphology change from a crystal structure point of view.

Figure 5 shows the excitation and emission spectra of $KEu(MoO_4)_2$ and $HEu(MoO_4)_2$. The excitation spectrum of $KEu(MoO_4)_2$ phosphor shows a broad O^{2-}-Mo^{6+} charge transfer (CT) band and some strong narrow peaks were observed between 360 and 500 nm, and were attributed to the f-f transitions of the Eu^{3+} ion. In addition, it is noted that the CT band of Eu^{3+}-O^{2-} is not clearly observed in the excitation spectra due to the possible overlap of the CT band with that of molybdate group [20-22]. On the other hand, $HEu(MoO_4)_2$ phosphor prepared by the H^+ exchange of $KEu(MoO_4)_2$, the excitation absorption band of the CT transition of O^{2-}-Mo^{6+} shifts to the longer wavelength side with H^+-exchanging and the excitation absorption band of the CT band of Eu^{3+}-O^{2-} is clearly observed in the excitation spectra. The excitation peak shift with H^+ exchanging can be explained by the change of the interaction with the environment around the Mo^{6+} ion in the host lattice.

In the emission spectra, meanwhile, all peaks corresponded to the Eu^{3+} 4f-4f transition, and the emission peak profiles of these sample before or after H^+-exchanging were essentially the same and there is no spectral shift due to the H^+-exchanging because the symmetric environment around the Eu^{3+} ion in the $(Eu(MoO_4)_2)_n$ layers is the same in the samples.

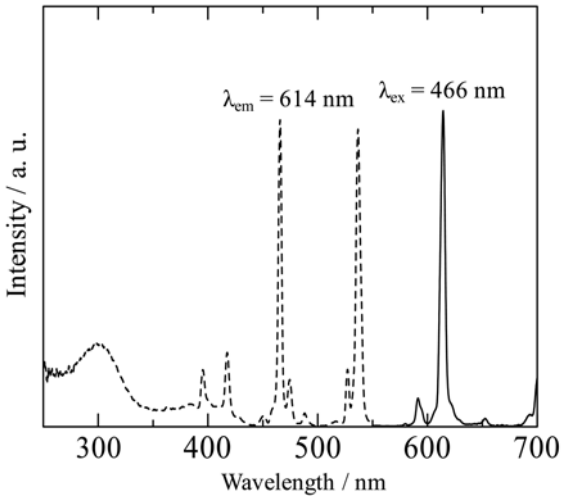

Fig. 6. Photoluminescence excitation and emission spectra of the $HEu(MoO_4)_2$ nanophosphor solution.

Figure 6 shows the excitation and emission spectra of the $HEu(MoO_4)_2$ nanophosphor solution, in which the concentration of the $HEu(MoO_4)_2$ phosphor powder was adjusted 9.76×10^{-3} mol/dm^3. Although the peak intensity of excitation and emission spectra of the phosphor solution was lower than that of the phosphor powder, similar to the results obtained for the $HEu(MoO_4)_2$ phosphor powder shown in Fig. 5. The excitation spectrum consisted of two broad band, corresponding to charge transfer (CT) transitions of Eu^{3+}-O^{2-} and O^{2-}-Mo^{6+}, respectively. Several strong narrow peaks were attributed to 4f-4f transitions of Eu^{3+}. Among these, the dominated sharp peak at 465 and 531 nm corresponded to the $^7F_0$-$^5D_2$ and $^7F_0$-$^5D_1$ transition of Eu^{3+}. In addition, the phosphor solution presents strong red-emission under excitation wavelength at 465 nm due to the 4f-4f transition of Eu^{3+}.

Conclusions

The $HEu(MoO_4)_2$ nanophosphor was synthesized for the first time by the H^+-exchange of $KEu(MoO_4)_2$ in 0.01 M aqueous HNO_3 solution at room temperature for 7 day. The nanophosphor obtained in the present study adopt the triclinic $KEu(MoO_4)_2$ structure in a single phase form, and the obtained $HEu(MoO_4)_2$ phosphor has rod-like particle morphology and the nanorod particle are 0.5-20 μm in length, and most have outer diameters ranging from 50 to 400 nm. The $HEu(MoO_4)_2$ nanophosphor exhibited excellent optical absorption at 465 and 531 nm, and presents strong red-emission due to the 4f-4f transition of Eu^{3+}. In addition, the $HEu(MoO_4)_2$ solution also show good luminescence efficiency under excitation at 465 nm. Since the $HEu(MoO_4)_2$ nanophosphor solution is transparent and show good luminescent emission, it is expected to use in crystal Si solar cells as a down-conversion materials.

References

1. Z. Zhang and Y. Wang, J. Electrochem. Soc. 154 (2007) J62-J64.
2. T.S. Chan, R.S. Liu, I. Baginskiy, N. Bagkar, and B.M. Cheng, J. Electrochem. Soc. 155 (2008) J284-J286.
3. Z.J. Zhang, S. Chen, J. Wang, X.X. Yang, J.T. Zhao, Y. Tao, H.H. Chen, and Y. Huang, Opt. Mater, 32 (2009) 99-103.
4. P. Zhang, L.X. Li, M.X. Xu, and L. Liu, J. Alloys Compd. 456 (2008) 216-219.
5. D.T.M. Huong, N.H. Nam, L.V. Vu, and N.N. Long, J. Alloys Compd. 537 (2012) 54-59.
6. M.N. Huang, Y.Y. Ma, X.Y. Huang, S. Ye, and Q.Y. Zhang, Spectrochim. Acta Part A: Mol. Biomol. Spectrosc. 115 (2013) 767-771.
7. U. Rambabu and S.D. Han, Ceram. Int. 39 (2013) 1603-1612.
8. J.Y. Chen, C.K. Huang, W.B. Hung, K.W. Sun, and T.M. Chen, Sol. Energy Mater. Sol. Cells 120 (2014) 168-174.
9. A. Luque and A. Martí, Phys. Rev. Lett. 78 (1997) 5014-5017.
10. V. Sivakumar and U.V. Varadaraju, J. Electrochem. Soc. 152 (2005) H168.
11. Y. Iso, S. Takeshita, and T. Isobe, J. Electrochem. Soc. 159 (2009) 72.
12. V.D. Rodríguez, J. Méndez-Ramos, V.K. Tikhomirov, J. del-Castillo, A.C. Yanes, and V.V. Moshchalkov, Opt. Mater. 34 (2011) 179-182.
13. S. Misra, L. Yu, M. Foldyna, and P.R.I. Cabarrocas, Sol. Energy Mater. Sol. Cells, 188 (2013) 90-95.
14. H. Hara, S. Takeshita, T. Isobe, T. Sawayama, and S. Niikura, Mater. Sci. Eng. B 178 (2013) 311-315.
15. H. Seo, Y. Wang, G. Uchida, K. Kamataki, N. Itagaki, K. Koga, and M. Shiratani, Electrochem. Acta, 95 (2013) 43-47.
16. H. Lian, Z. Hou, M. Shang, D. Geng, Y. Zhang, and J. Liu, Energy, 57 (2013) 270-283.
17. S. Takeshita, T. Isobe, T. Sawayama. and S. Niikura, Prog. Cryst. Growth. Charact. Mater. 57 (2011) 127-136.
18. P.V. Klevtsov and R.F. Klevtsova, J. Struct. Chem. 18 (1977) 339-355.
19. K. Momma and F. Izumi, J. Appl. Cryst. 41 (2008) 653-658.
20. L. Luan and Y. Xu, Appl. Phys. A 94 (2009) 365-371.
21. A. Xie, X. Yuan, F. Wang, Y. Shi, J. Liu, and Z. Mu, J. Alloys Compd. 501 (2010) 124-129.
22. W.L. Feng, Y. Jin, Y. Wu, D.F. Li, and A.K. Cai, J. Lumin. 134 (2013) 614-617.